Macromolecules

Article

pubs.acs.org/Macromolecules

Characterization of Block Copolymer Self-Assembly: From Solution to Nanoporous Membranes

Liat Oss-Ronen,[†] Judith Schmidt,[†] Volker Abetz,[‡] Aurel Radulescu,[§] Yachin Cohen,[†] and Yeshayahu Talmon*,[†]

[†]Department of Chemical Engineering, Technion-Israel Institute of Technology, Haifa 32000, Israel

[‡]Institute of Polymer Research, Helmholtz-Zentrum Geesthacht, 21502 Geesthacht, Germany

[§]Jülich Centre for Neutron Science, Forschungszentrum Jülich GmbH, Outstation at FRM II, 85747 Garching, Germany

Supporting Information

ABSTRACT: Self-assembly of isoporous membranes of polystyrene-*b*-poly(4-vinylpyridine) (PS-*b*-P4VP) involves many parameters: the block copolymer composition, the solvent and its interactions with the respective blocks, composition of the casting solution, solvent evaporation, and immersion into a water bath. We characterized the self-assembly of PS-*b*-P4VP in solution in nearly neutral or P4VP-selective solvent and on the surface of a cast film. We used a combination of room temperature (RT) and cryogenic high-resolution scanning electron microscopy (cryo-HR-SEM) to study copolymer micellization in dried films, in solution, and on the membrane surface during evaporation. The solutions, with and without addition of small water amounts, were investigated by cryogenic transmission electron microscopy (cryo-TEM) and small-angle neutron scattering (SANS). We have shown that the starting point for membrane formation is a microphase-separated copolymer solution with the P4VP within the micelle core. As water is introduced, this structure is preserved as long as the system is far from equilibrium. Closer to equilibrium the PS blocks form the micelles core.

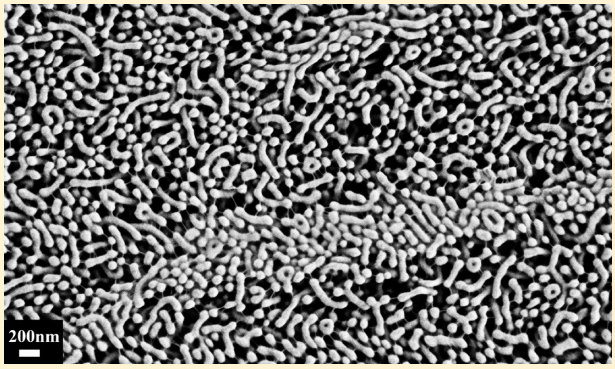

INTRODUCTION

Self-assembly of block copolymers in solution has been a topic of immense interest both for the fundamental aspects by which the size, shape, and arrangement of highly appealing nanoscopic structures can be tuned by molecular structure, solvent interactions, and processing conditions[1−3] and for a growing variety of practical applications.[4] Particular interest has been focused recently on nanoporous membranes,[5,6] fabricated via block copolymer self-aggregation, providing a dense assembly of pores with a narrow size distribution, in a scalable solution casting processes. Previous studies demonstrated an innovative and simple "one-step" method to prepare such isoporous membranes by casting a solution of the diblock copolymer polystyrene-*b*-poly(4-vinylpyridine), PS-*b*-P4VP.[7] Composite integral asymmetric structures were prepared using a combination of solvent evaporation and nonsolvent-induced phase separation.[7−11] Using this methodology, similar membranes of polystyrene-*b*-poly(2-vinylpyridine), PS-*b*-P2VP, could be prepared.[8] Those are similar in concept to asymmetric membranes in current practical usage, whereby a thin separation layer of ordered pores evolves integrally on a layer of disordered pores, which gradually increase in size. That thin asymmetric film rests on a nonwoven support. Membranes prepared in this manner exhibit both high flux and selectivity[7−9,11] and, moreover, could be controlled by variation of pH.[9−11]

Formation of the isoporous membrane structure during casting is a complex process, which depends on several parameters. The equilibrium state of the copolymer solution prior to casting is a primary issue. The effects of changes in solution concentration and solvent selectivity during partial or full solvent evaporation set the initial stage of the emerging structural features, in particular when a volatile solvent component is used.[7] Much attention has been devoted to the required orientation of the cylindrical pore-forming domains perpendicular to the membrane plane, which may be achieved by proper solvent evaporation,[12−14] as has been modeled recently.[15] Immersion in a nonsolvent (water) yields the final asymmetric structure during the transformation from the liquid to the solid state, a process referred to as "phase inversion" in the membrane fabrication literature.[16,17]

It is important to understand the nature of the initial aggregation in the block copolymer solution, as it is there that the pore forming domains originate. Microphase separation of

Received: July 31, 2012
Revised: November 4, 2012
Published: December 5, 2012

   dx.doi.org/10.1021/ma301611c | *Macromolecules* 2012, 45, 9631−9642

domains rich in the minority block has been invoked as the pore-formation mechanism in some systems. This may be induced by several effects such as an increase in solution concentration due to solvent evaporation or by a change in solvent selectivity due to evaporation of a volatile additive or addition of a nonsolvent (often termed "nonsolvent-induced phase separation"). Often, the minority component needs to be subsequently removed to yield the desired pores.[5] Variation of polymer−solvent interactions and increasing solvent selectivity are known to control the structure of the micelles and their ordered packing.[18,19] Obviously, for the purpose of membranes for water treatment, hexagonal packing of cylindrical micelles perpendicular to the membrane plane is the desired structure.

The unique initial conditions that have been employed for formation of isoporous membranes made of PS-*b*-P4VP by the simple one-step process[7−9] included high molecular weight polymer (over 150 kDa) containing about 15−20 wt % P4VP (molecular percentage is rather similar due to almost similar molecular weights of the repeating units of PS and P4VP) and high polymer concentration (about 20 wt %) in a solvent mixture of *N*,*N*-dimethylformamide (DMF) and tetrahydrofuran (THF) at 70/30 wt ratio. The state of micellization under such conditions had not been tested before.

Evaluating the state of micellization is relevant to delineation of the pore-formation mechanism during membrane casting, which may provide better design and control of the pore structure. The first publication on the isoporous PS-*b*-P4VP membranes[7] suggested that the mechanism of pore formation is due to assembled copolymer micelles having P4VP in their core during THF evaporation from solution. Other publications[9,11] challenged this mechanism and suggested that micelles having the majority PS component in their core are the ones to assemble during the casting process and that these micelles pack on a two-dimensional honeycomb−hexagonal lattice (3*m* point group symmetry for the micelles) rather than on the usual triangular−hexagonal lattice (6*mm* point group symmetry for the micelles). This lower symmetry packing is required so that the "missing" micelles in the middle of the hexagons can be the origin of the membrane pores, with P4VP on their inner side. No apparent reason is provided for such lower symmetry packing, although stochastically driven systems, such as phase separation far from equilibrium, may exhibit spontaneous symmetry breaking.[20]

It is therefore the objective of this study to evaluate the state of micellization in the PS-*b*-P4VP solutions, from which isoporous membranes are cast by the simple "one-step" process, and the structural transformations that take place upon exposure to water. The main premises of this research are to investigate the systems as close as possible to their native state, with minimal perturbation by sample preparation, and to provide a comprehensive evaluation by combining direct imaging electron microscopy techniques with validation by scattering methods. Direct imaging of solvent-containing soft matter by electron microscopy requires cryogenic techniques that vitrify the structure to prevent molecular motion and solvent evaporation. Cryo-transmission electron microscopy (cryo-TEM) allows direct imaging of vitrified thin films of liquid systems.[21,22] For the study of bulk samples rather than thin films, cryogenic high-resolution scanning electron microscopy (cryo-HR-SEM) can be applied, whereby the liquid-containing sample is rapidly vitrified and fractured, and the structure of the fracture surface is imaged. Alternatively, the surface of the fast-cooled specimen is imaged. In cryo-SEM specimens contrast may be enhanced by selective etching (sublimation) from the observed surface.[23]

Measurements of the small-angle scattering of X-rays and neutrons (SAXS, SANS) have been used extensively to study several aspects of block copolymer solutions, such as the shape, size, and packing of block copolymer micelles, the nature of ordered structures, determination of phase diagrams, and detailed assessment of the order−disorder and order−order transitions.[18,24−26] In particular, SANS with contrast variation[27] has been usefully applied to study the solvent distribution between the phase-separated structures in block copolymer solutions,[28,29] and microphase separation induced by a differentiating nonsolvent.[30] In the present study we apply direct imaging by cryo-TEM and cryo-HR-SEM combined with contrast variation SANS to evaluate the nature of the micelles formed in the high-MW block copolymer solutions in solvents that are nearly neutral or selective for the minority block and the transitions that occur by addition of a nonsolvent (water), as in fabrication of isoporous membranes, to elucidate the mechanism of pore formation.

EXPERIMENTAL SECTION

Materials. We used polystyrene-*b*-poly(4-vinylpyridine) (PS-*b*-P4VP) copolymers, synthesized at the Institute of Polymer Research, Helmholtz-Zentrum Geesthacht, using the same methodology as described before.[7] Specifically, we used the following copolymers (numbers in subscript indicate the weight percent of each block): PS_{82}-*b*-$P4VP_{18}$, 129 kg/mol; PS_{78}-*b*-$P4VP_{22}$, 153 kg/mol; PS_{73}-*b*-$P4VP_{27}$, 310 kg/mol; dPS_{85}-*b*-$P4VP_{15}$, 388 kg/mol (PS fully deuterated). Copolymers were dissolved in mixtures of tetrahydrofuran (THF, Frutarom, Haifa, Israel) and *N*,*N*-dimethylformamide (DMF, Frutarom, Haifa, Israel) or fully deuterated THF (THF-d_8) and fully deuterated DMF (DMF-d_7), both from Sigma-Aldrich, St. Louis, MO.

Cryogenic Temperature Transmission Electron Microscopy (Cryo-TEM). We imaged relatively low-concentration solutions by cryo-TEM. For sample preparation, we used a controlled environment vitrification system (CEVS), held at 25 °C. The environment of the system was saturated with the solvents of the specific solution used or with water. We applied a drop of the solution onto a perforated carbon film, supported by a TEM copper grid, and blotted the drop to form a thin film of the solution. The sample was immediately plunged into liquid nitrogen (LN_2) and kept at cryogenic conditions during transfer into the microscope and during imaging. The cryogen of choice, liquid ethane, dissolves most organic solvents. However, the less effective cryogen, LN_2, is sufficient to vitrify most organic solvents.[31] We used an FEI Tecnai T12 G^2 TEM, operated at 120 kV and low-dose mode.[32] Samples were loaded onto a 626 Gatan cryo-holder and kept at −175 °C during imaging. Images were recorded digitally by a Gatan high-resolution US1000 cooled-CCD camera.

High-Resolution Scanning Electron Microscopy (HR-SEM). We characterized dried films, and more concentrated solutions, by room-temperature and cryogenic-temperature HR-SEM, respectively. Dried samples for HR-SEM were prepared from PS_{82}-*b*-$P4VP_{18}$, 129 kg/mol, solutions in 70%/30% DMF/THF weight ratio. A drop of the solution was cast on a silicon wafer. The sample was then left overnight in a closed environment of air saturated with water for a high-humidity environment. Finally, the samples were dried overnight in a vacuum oven operated at room temperature. In other cases, we immersed films produced from 20% copolymer solutions in Milli-Q distilled water 10 s after casting and left them in water overnight before vacuum oven drying.

Cryo-HR-SEM specimens were prepared in a similar CEVS as described above. Each kind of specimen, having a specific solution composition, was prepared at least twice. A drop of the solution (PS_{78}-*b*-$P4VP_{22}$, 153 kg/mol, or PS_{73}-*b*-$P4VP_{27}$, 310 kg/mol in DMF/THF) was inserted between two gold planchettes. The sample was held by a

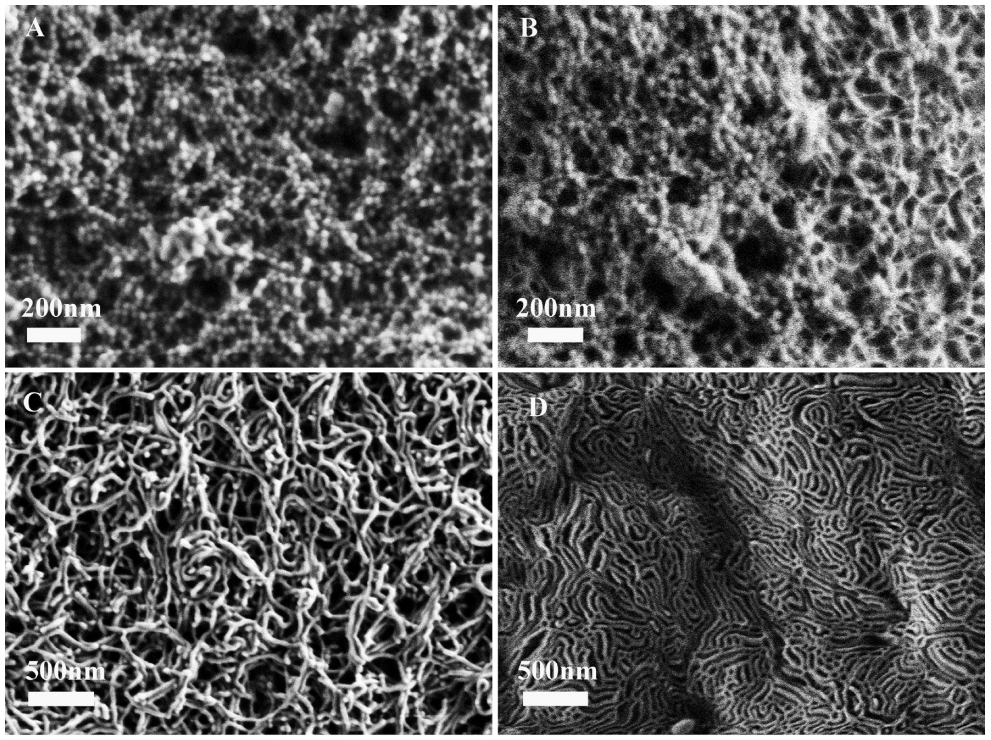

Figure 1. Room-temperature HR-SEM of PS_{82}-*b*-$P4VP_{18}$, 129 kg/mol, dried block copolymer films prepared from solutions in 70%/30% DMF/THF: (A) 5% copolymer in original solution; (B) 10% copolymer; (C) 20% copolymer; (D) 20% copolymer; film was immersed into water after casting.

specially designed tweezers, which were plunged into liquid nitrogen immediately after preparing the specimen. We then transferred it under cryogenic conditions into a BAL-TEC BAF 060 freeze-fracture-replication system. While under vacuum and at −180 °C, the sample "sandwich" was quickly opened to fracture the vitrified solution. The fractured surface was usually lightly etched by heating the specimen stage to −100 °C and cooling back and was also usually coated with 4 nm of Pt/C. A detailed description of the cryo-HR-SEM methodology is given by Issman and Talmon.[23]

Membranes were vitrified during the casting procedure for cryo-HR-SEM observation. A 20% PS_{73}-*b*-$P4VP_{27}$, 310 kg/mol, in 70%/30% DMF/THF solution was cast on a polyester nonwoven support pretreated with THF. The membrane was then left to dry for measured times and immersed into liquid nitrogen for vitrification.[7,33] We mounted the membrane onto a specially designed stub for cryo-HR-SEM imaging of its surface, and transferred it under cryogenic conditions into the BAL-TEC BAF 060 freeze-fracture-replication system. The membrane surface was lightly etched by heating the specimen stage to −100 °C, and cooling back to about −180 °C, and was coated with 4 nm of Pt/C. Finally, the sample was transferred into the HR-SEM under cryogenic conditions and high vacuum. For comparison with the dried state of the membranes, a piece of the membrane was left to dry overnight at RT, and then dried in a vacuum oven, before HR-SEM imaging.

All HR-SEM samples were observed with a Zeiss Ultra-Plus HR-SEM equipped with a BalTec VCT-100 cryo-stage. The cryo-stage was kept at −145 °C during cryo-HR-SEM imaging. Samples were imaged at a low accelerating voltage of 1 kV, using a combination of two secondary electron detectors: an Everhart-Thornley detector and/or a high-resolution in-the-column detector.

Small-Angle Neutron Scattering (SANS). Solutions for SANS characterization were prepared from 5% PS_{73}-*b*-$P4VP_{27}$, 310 kg/mol or dPS_{85}-*b*-$P4VP_{15}$, 388 kg/mol (PS fully deuterated), in mixtures of THF, DMF, THF-d_8, and DMF-d_7. SANS measurements were conducted on the KWS-2 beamline at the Jülich Center for Neutron Science at the FRM-II reactor, TU München. Measurements were performed at 18 °C, using 2, 8, and 20 m sample-to-detector distances, at 4.8 Å wavelength. Contrast variation was employed to evaluate the location of the PVP and PS blocks in the emerging structures.[27]

RESULTS AND DISCUSSION

Amphiphilic block copolymers tend to microphase-separate in solution as a function of various parameters, including polarity of each block, molecular architecture of the copolymer, molecular interactions between the blocks, solvents used, and solution composition.[34] In our research we studied the self-assembly of PS-*b*-P4VP linear block copolymers as a function of solution composition. In the studied polymer the nonpolar PS chains were longer than the polar P4VP chains. It was dissolved in a mixture of solvents containing DMF and THF. Such solutions had been used for casting isoporous membranes on the nanometric scale.[7,33] Finally, we investigated the effect of small added amounts of water.

First we characterized a set of dried samples that were made from solutions in 70%/30% DMF/THF weight ratio, containing increasing concentrations of PS_{82}-*b*-$P4VP_{18}$, 129 kg/mol: 5%, 10%, 15%, 20%, and 25%. Each solution was cast as a thin film on a silicon wafer and was left overnight in a high-humidity environment, followed by drying in a vacuum oven. With increased copolymer concentration, we observed a transition from spherical micelles (5% copolymer, Figure 1A) to a combination of spherical micelles with a network of threadlike micelles (TLMs, 10% copolymer, Figure 1B) and to a TLM network alone (20% copolymer, Figure 1C). This network became denser, and more branched, when we immersed the film into distilled water immediately after casting (Figure 1D). Hence, in this case increasing the polymer concentration led to elongation of the micelles, until a network of TLMs was formed. However, these micelles were observed

dx.doi.org/10.1021/ma301611c | *Macromolecules* 2012, 45, 9631−9642

after drying a cast film and not in solution. Drying may significantly affect self-assembly of these structures.

To image the morphology in solution, we used cryo-HR-SEM of vitrified copolymer solutions. We prepared block copolymer solutions (PS_{78}-*b*-$P4VP_{22}$, 153 kg/mol, and PS_{73}-*b*-$P4VP_{27}$, 310 kg/mol) in a composition used for membrane casting: 20% copolymer in a solution of 70%/30% DMF/THF weight ratio.[7] Cryo-HR-SEM allowed us to observe directly the morphologies in those viscous solutions without staining or drying. In all cases (Figure 2), the vitrified and fractured sample was warmed to −100 °C for 5 s and cooled back to −180 °C, for slight sublimation of the solvents from the surface of the specimen ("etching"), before transferring it into the HR-SEM.

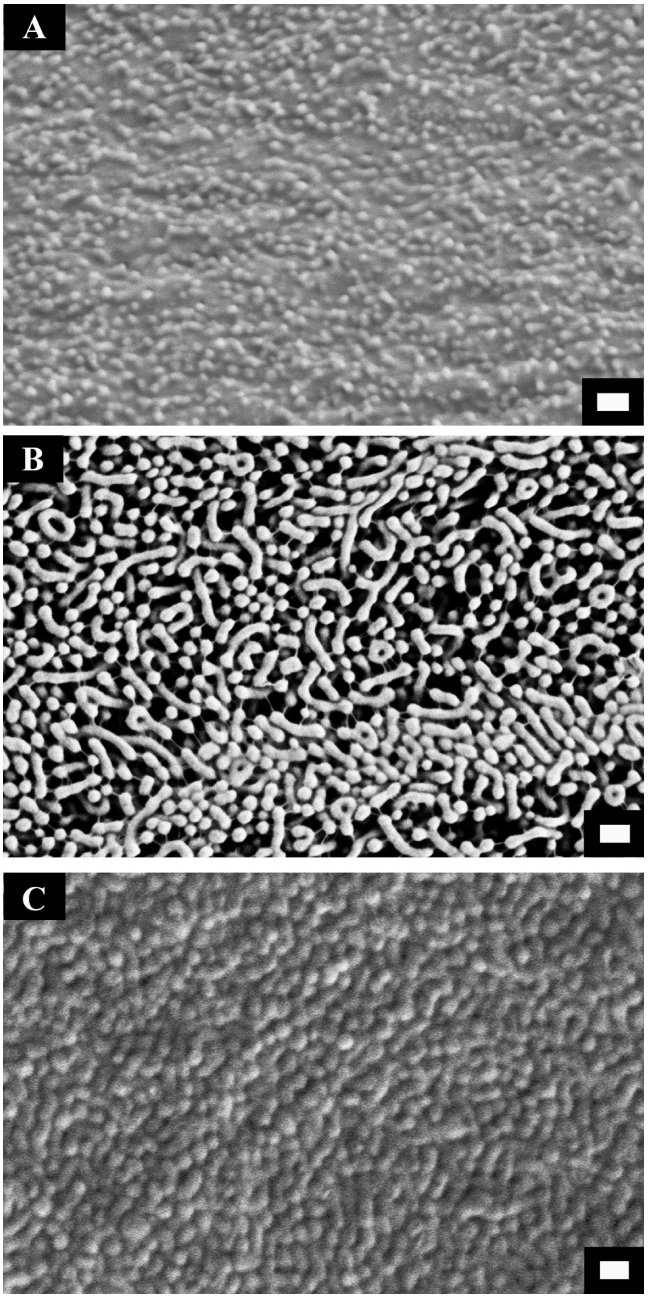

Figure 2. Cryo-HR-SEM of solutions of 20% block copolymer in 70%/30% DMF/THF: (A) PS_{78}-*b*-$P4VP_{22}$, 153 kg/mol, fine etching; (B) PS_{78}-*b*-$P4VP_{22}$, 153 kg/mol, deep etching; (C) PS_{73}-*b*-$P4VP_{27}$, 310 kg/mol. Bars are 200 nm.

This allowed us to expose the morphology of the nanostructures in the solution. The differences in appearance between the three images of Figure 2 are a result of different quantities of solvents sublimed from the surface of the fractured sample, before its transfer to the HR-SEM. In some cases this sublimation was insufficient to fully expose the structures (Figure 2A), and only hints of the morphology were observed. In other cases (Figure 2B), a larger portion of the solvents was sublimed, exposing mainly spherical and short TLMs. Figure 2C presents a solution of a composition similar to those of Figures 2A and 2B with a copolymer about twice as large in molecular weight (310 kg/mol compared with 153 kg/mol). Mainly spherical micelles and short TLMs are observed in this system as well, their dimensions being larger due to the higher molecular weight. In Figure 2B, we also see some short TLMs that formed rings or junctions; all had swollen end-caps. This behavior is typical of micelles formed by amphiphilic molecules or copolymers and is explained by different free energies for molecules in the cylindrical body, in end-caps, and in junctions.[35,36]

Microphase separation into micelles in the starting solution used for membrane casting is expected for linear block copolymers of sufficiently high molecular weight and concentration; the presence of micelles may be relevant to membrane structure formation. A model presented by Phillip et al.[15] for a similar system demonstrated microphase separation during solvent evaporation in the cast solution, followed by orientation of the emerging micelles perpendicularly to the cast membrane plane, due to effects of solvent evaporation rate, film thickness, and other parameters. Our results show that in the present system the copolymer forms micelles already in the original casting solution.

Following imaging of the equilibrium aggregates in solution, we used the same cryo-HR-SEM methodology to observe morphologies in a set of samples that simulated the first steps of the membrane casting process to study the evolution from nanostructures in solution into membrane pores. The membrane casting process, according to Peinemann et al.[7] and Fierro et al.,[33] with some small changes, involves the following steps: (1) casting a thin uniform film of the copolymer solution onto a pretreated support; (2) letting the solvents evaporate for a given time (a few seconds to a few minutes, depending on the system composition); (3) immersing the film into a nonsolvent (water) bath. Since THF is the more volatile solvent, we expect that during the evaporation step THF concentration on the surface of the cast film decreases, until a solution of the copolymer in DMF with very small THF concentration remains. To mimic the process and see how structures evolve during this step, we prepared a set of solutions with decreasing THF concentrations, while keeping the ratio between copolymer and DMF constant. The starting solution was 20% copolymer in 70%/30% DMF/THF weight ratio, as shown in Figure 2, and the final solution was 26.3% copolymer in DMF alone. The same set of solutions was prepared for two copolymers: PS_{78}-*b*-$P4VP_{22}$, 153 kg/mol, and PS_{73}-*b*-$P4VP_{27}$, 310 kg/mol. Results obtained by cryo-HR-SEM (Figure 3) showed a transition from spherical and short TLMs (as shown in Figure 2) to mainly TLMs, as the THF concentration decreased. However, the differences between the samples shown in Figure 3 were not dramatic.

The transition to longer TLMs as the THF concentration decreases may suggest the process whereby cylindrical pores are formed on the top layer of membranes.[7] The length of these

dx.doi.org/10.1021/ma301611c | *Macromolecules* 2012, 45, 9631−9642

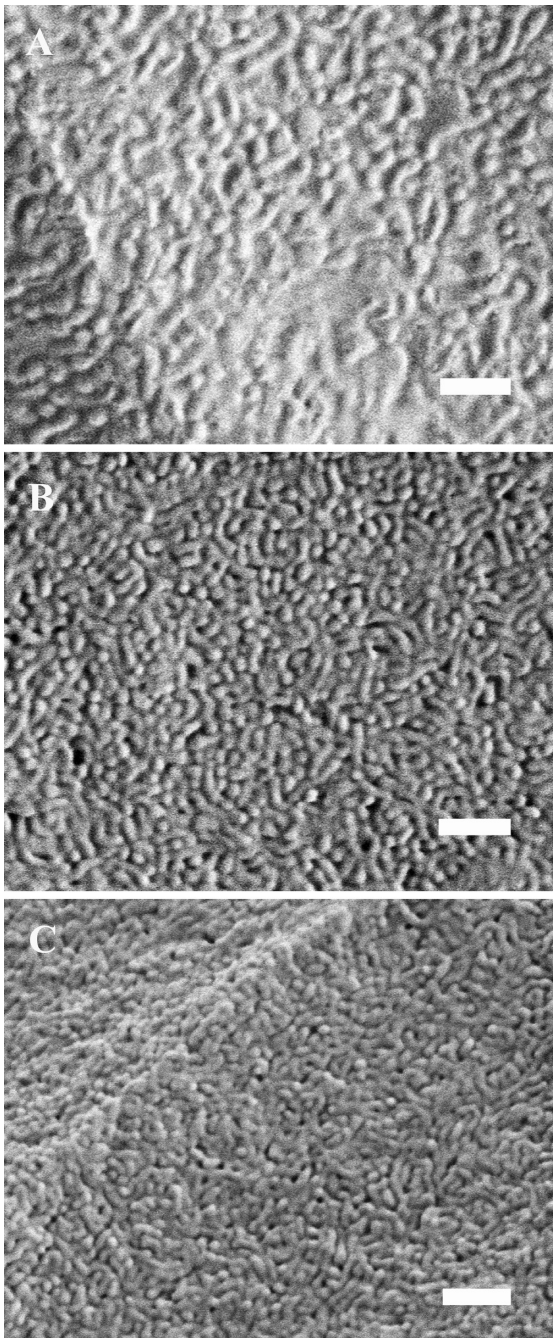

Figure 3. Cryo-HR-SEM of copolymers PS_{73}-*b*-$P4VP_{27}$, 310 kg/mol (A), and PS_{78}-*b*-$P4VP_{22}$, 153 kg/mol (B, C), in solutions with different THF/DMF weight percent ratios: (A) 21.8% copolymer in 22%/78%; (B) 23.7% copolymer in 13%/87%; (C) 26.3% copolymer in 100% DMF. Bars are 500 nm.

cylinders depends on the block copolymer used, the composition of cast solution, and the casting conditions. However, the pores were formed in an ordered manner perpendicular to the surface of the film, while the TLMs we observed in the set of solutions were not ordered in any direction. It has been shown that cylinder orientation during membrane casting can be due to rapid solvent evaporation from the thin cast film, which is directed perpendicular to the surface, hence forming a solvent concentration profile in that direction.[15] The effect of water concentration gradient perpendicular to the interface of cast solutions should also be considered.

We also used cryo-HR-SEM to study morphology evolution on the top surface of membranes *in situ*, namely, during their casting process. We followed the first two steps of the casting process described above[7,33] and vitrified the membrane after increasing times of solution evaporation. In this case, a solution of 20% PS_{73}-*b*-$P4VP_{27}$, 310 kg/mol, in 70%/30% DMF/THF weight ratio was used. After vitrification, the sample was kept in high vacuum at −180 °C, and a thin solvent layer was sublimed from its top surface to expose the morphology better. That was done by raising the temperature of the sample to −100 °C for ∼5 s (Figure 4D) or for 1 min (Figure 4A−C) and cooling back to about −180 °C. Following this brief sublimation procedure, the sample was transferred into the HR-SEM under cryogenic conditions and in high vacuum. After 11 s of evaporation during membrane casting, the micrograph showed spherical micelles that had been present in the original casting solution (Figure 4A). As the evaporation proceeded, the micelles became organized on the surface of the membrane and fused into a film covered with bumps (Figure 4B), which then collapsed into craters (Figure 4C). After 40 s of evaporation and more, the craters became pores (Figure 4D), resembling the pores in the final membrane (Figure 4E). Here is our explanation for this structure evolution: At short evaporation times (Figure 4A,B) the solvent still contains much of the more volatile THF, which is presumably present mainly in the PS-rich regions. During etching of the vitrified solution, THF is removed preferentially from these regions, revealing the P4VP-rich domains as globular micelles. Upon longer evaporation times (Figure 4C,D), DMF is also removed. The PS-rich regions become denser, as remaining DMF favors the P4VP domains, so that upon etching of the vitrified solution the latter regions appear as pits and finally as holes.

The methodology of cryo-HR-SEM presented here was developed in our lab recently and may be used for various applications.[23] A similar method of top surface cryo-SEM imaging was shown by Cardinal et al.[37] In the current project this method is a new tool to characterize pore formation as a function of membrane casting conditions and solution composition. The same method may also be used to study the effect of a nonsolvent (water) on surface morphology as a function of evaporation time.

The results presented above indicate that micelles are formed already in the polymer solution prior to membrane casting. However, they do not reveal which block resides in the micelle core and which is in the surrounding medium. It was shown in several studies that micelles formed in solution can be the progenitors of the final pores in membranes cast from these solutions, either by virtue of their hydrophilic nature, such as in films cast from polystyrene-*b*-poly(ethylene oxide) (PS-*b*-PEO),[13] or by being sacrificially etched, such as in polystyrene-*b*-polylactide (PS-*b*-PLA).[14] In the cases mentioned above, a PS-selective solvent is used and the micelle cores were formed by the minor block having less favorable solvent interactions. Which block forms the micelle core in solution of an asymmetric block copolymer strongly depends on the solvent composition and on its interaction with the two blocks. Micellization with the majority block forming the core can occur in a solvent that is strongly selective for the minority block, in what has been termed as "crew cut" micelles.[38] Furthermore, differences in solvent selectivity to one of the blocks also determine the size and solvent content within the

dx.doi.org/10.1021/ma301611c | *Macromolecules* 2012, 45, 9631−9642

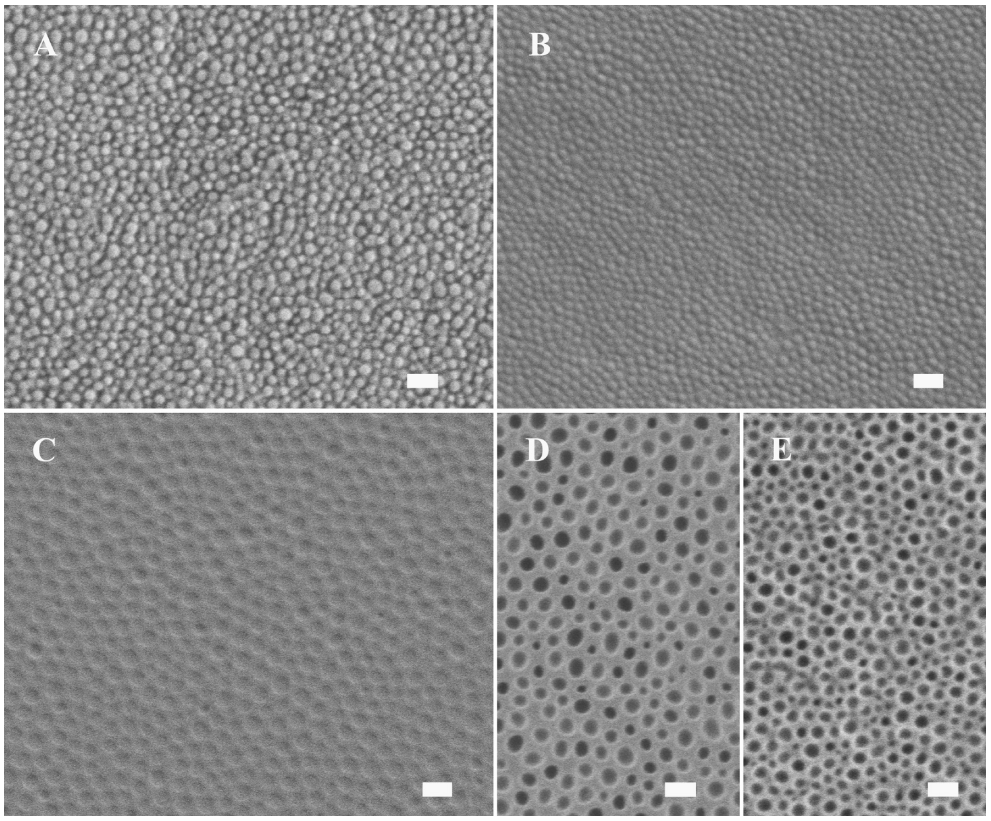

Figure 4. Cryogenic (A–D) and room temperature (E) HR-SEM of membranes prepared from 20% PS_{73}-*b*-$P4VP_{27}$, 310 kg/mol in 70%/30% DMF/THF: (A) 11 s evaporation time; (B) 18 s evaporation time; (C) 25 s evaporation time; (D) 40 s evaporation time; (E) a dried membrane. Bars are 200 nm.

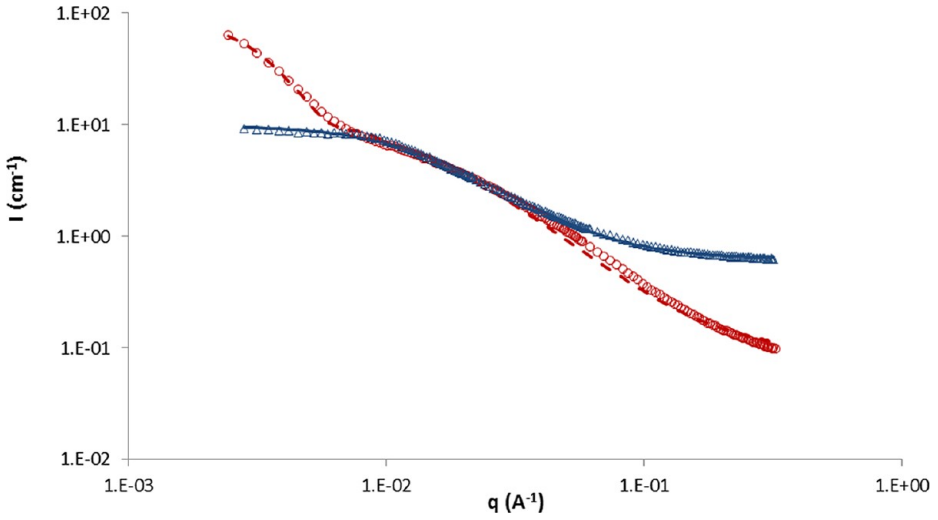

Figure 5. SANS patterns of 5% copolymer solutions: (○) PS_{73}-*b*-$P4VP_{27}$, 310 kg/mol in DMF-d_7 (full contrast); (△) dPS_{85}-*b*-$P4VP_{15}$, 388 kg/mol, in a mixture of 21%/79% (v/v) DMF-d_7/DMF (matching P4VP). Dashed and solid lines are model fits for the full contrast sample and for the P4VP-matched sample, respectively.

micelle core. For example, in the case of nearly symmetric PS-*b*-P4VP dissolved in a mixed toluene–ethanol solvent, hard and large spherical micelles were formed in highly selective solvent mixtures, while small and soft (solvent-swollen) ones were formed in less-selective solvent mixtures. Soft micelles were also formed in nearly neutral solvent mixtures at sufficiently high concentration.[39] Thus, micellization in BCP solution may be due to either unfavorable interactions between the solvent and one of the blocks or unfavorable interactions between the two polymer blocks even in a nonselective solvent.

In the present case, the mixed 70/30 DMF/THF solvent may be considered as nearly neutral for the PS–P4VP copolymer, whereas DMF is slightly selective for P4VP.[10] Some indication that microphase separation into spherical micelles with P4VP in their core should occur even in DMF may be obtained from a recent publication of the phase diagram of a model high-MW diblock copolymer in the semidilute state,

dx.doi.org/10.1021/ma301611c | *Macromolecules* 2012, 45, 9631–9642

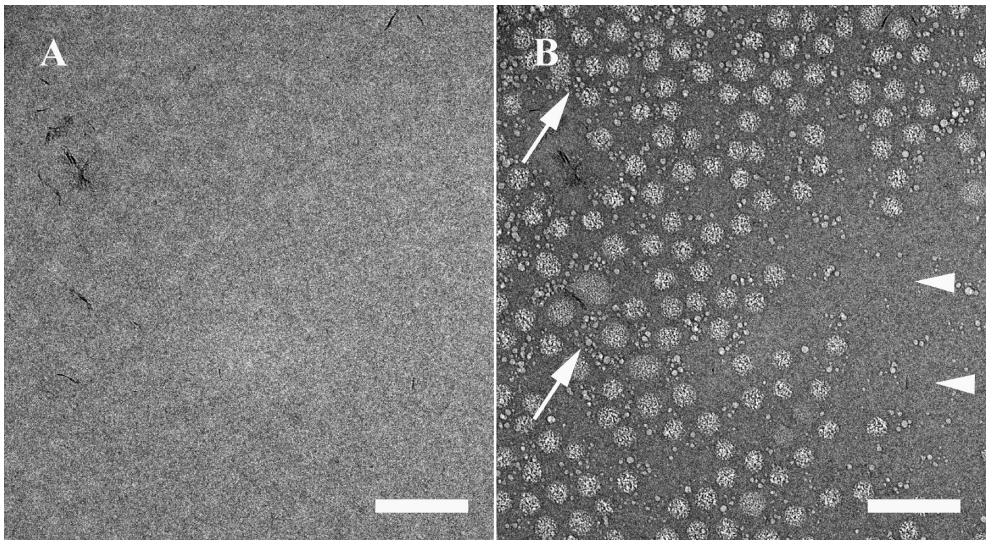

Figure 6. Cryo-TEM of 5% PS_{73}-*b*-$P4VP_{27}$, 310 kg/mol in DMF, after different electron exposures: (A) ~15 $e^-/Å^2$; (B) ~50 $e^-/Å^2$. Arrows and arrowheads point to differences between radiation damage in the solvent around micelles and far from micelles, respectively. Bars are 200 nm.

based on first-principles calculations.[40] The model assumes one block to be an ideal random chain, and the other a self-avoiding chain, and that the two blocks are mutually avoiding, with otherwise athermal interaction. This provides a reasonable reference point for PS-*b*-P4VP in DMF, as it is nearly a θ-solvent for PS in (Flory parameter $\chi \sim 0.5$),[41] while it is a good solvent for P4VP. The model predicts the critical micellization concentration (cmc) for the case of an asymmetric copolymer, with a fraction of the less-soluble block of 0.7 to be about 3 vol %.[40] This is an upper bound in this case, as the polymers have a repulsive interaction, with $\chi_{PS-P4VP}$ estimated to be above 0.3. The calculated phase diagram predicts that a semidilute solution of the copolymer under study is expected to be microphase separated into spherical micelles. By the common "lever rule", the micelles cores are formed by the minority phase. This indicates that under the conditions in our study microphase separation should lead to micelles containing the minority P4VP blocks in their core, although the solvent is selective for these blocks.

We studied the location of each block of the copolymer in the solution, as well as the effect of water addition into the system, using a combination of two complementary methods: SANS and cryo-TEM. Cryo-TEM provided direct images of the aggregates in solution, while SANS helped us to model and add quantitative data to this information. We characterized block copolymer solutions of lower concentrations (5%), with and without addition of small amounts of water. Lower copolymer concentrations were used to decrease the viscosity of the samples and allowed us to apply the methods mentioned above. We used only DMF as the solvent for two reasons. Although the initial solution is in mixed DMF/THF, the membrane casting process involves a solvent evaporation stage, which is expected to remove a significant amount of THF, which is much more volatile. In addition, we seek to show that the P4VP blocks are in the micelle core even in its more selective solvent, DMF. SANS patterns from samples made of 5% PS_{73}-*b*-$P4VP_{27}$, 310 kg/mol, or dPS_{85}-*b*-$P4VP_{15}$, 388 kg/mol (PS fully deuterated), in DMF (fully deuterated or a mixture of hydrogenated and deuterated) are shown in Figure 5. Here we used the contrast matching method to find the position of each block of the copolymer in the structures that were formed in solution. Matching the scattering length densities (SLD) of the solvent to that of the polymer blocks masked structures that were formed by that block.[27] The solid line in Figure 5 shows clearly that matching the solvent SLD to that of hydrogenated P4VP eliminates the excess scattering at low angles, observed at full contrast. Such a curve is typical for semidilute polymer solutions, without micellar structures. Conversely, at full contrast (fully hydrogenated polymer in fully deuterated solvent), we observed significant excess scattering at low angles, as expected from micellar structures (dashed line). Similar results were obtained for the same copolymer with a solvent mixture of 70%/30% DMF-d_7/THF-d_8 (see Supporting Information). The comparison between the two curves indicates that the micellar structure is due to P4VP, not to PS, meaning that the micelles core is made of the P4VP blocks, while their shell is composed of PS blocks as a semidilute polymer solution in DMF.

To quantitatively fit the experimental data, we used a combination of two models: a semidilute polymer solution model[42] and a system of monodisperse spheres (eq 1).[43] Since the inner volume within the micelles may be seen also as a confined semidilute solution of P4VP, in final fitting of the experimental data, using the functional form given in eq 1, we added a third term for the inner-micelle semidilute solution. Linear additivity of the functional forms for the micellar shape and its inner structure was shown to be valid when the length scale of the inner structure is much smaller than the micelle radius.[44] The scattering pattern at full contrast is thus fitted by

$$I(q) = I_{0,1}\left(3\frac{\sin(Rq) - Rq\cos(Rq)}{(Rq)^3}\right)^2 + I_{0,2}\left(\frac{1}{1 + a_1^2 q^2}\right) + I_{0,3}\left(\frac{1}{1 + a_2^2 q^2}\right) + B \quad (1)$$

where $q = (4\pi/\lambda)\sin\theta$ is the scattering vector, λ is the neutron wavelength, 2θ is the scattering angle, $I(q)$ is the scattering intensity, and B is the incoherent scattering background. The first term of the model is due to scattering by spherical micelles, where $I_{0,1}$ is the intensity coefficient and R is the sphere radius. The two Lorentzian functions represent the semidilute P4VP/

dx.doi.org/10.1021/ma301611c | *Macromolecules* 2012, 45, 9631−9642

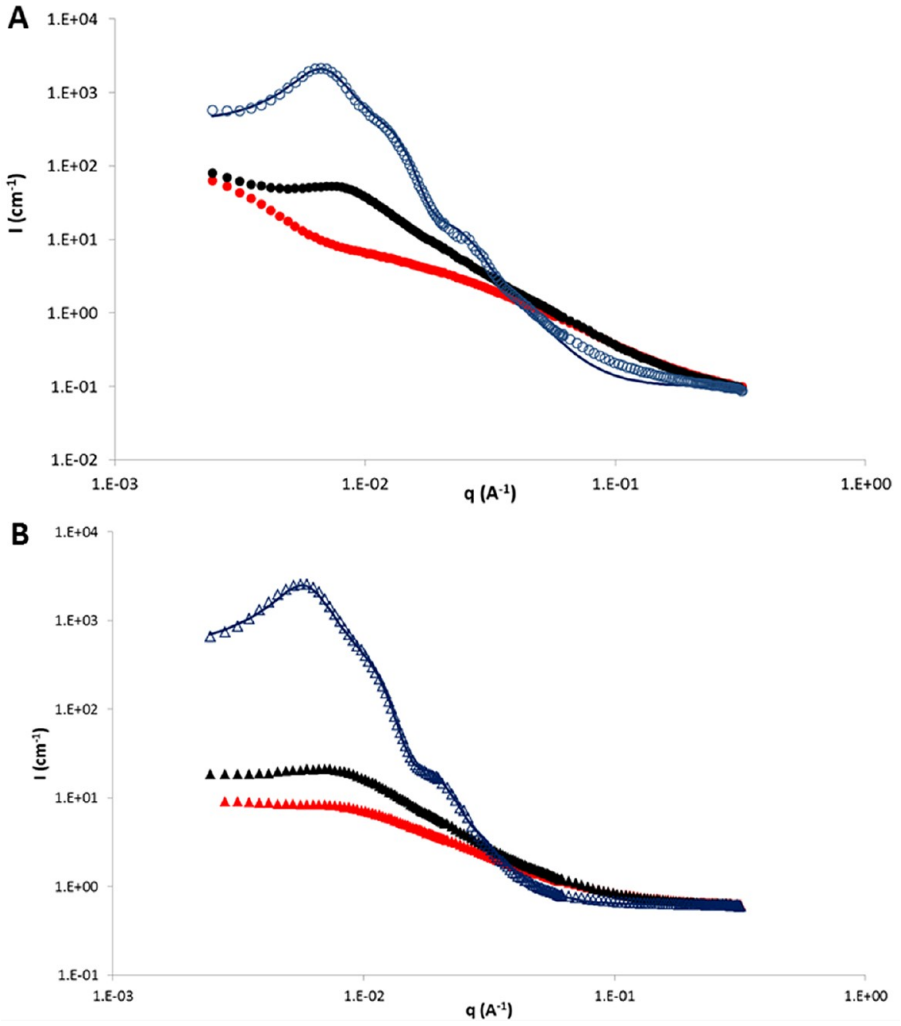

Figure 7. SANS patterns of 5% copolymer solutions with additions of water: (A) PS_{73}-*b*-$P4VP_{27}$, 310 kg/mol in DMF-d_7: red ●, no water addition; black ●, 1.2% D_2O addition; ○, 3.7% D_2O addition. (B) dPS_{85}-*b*-$P4VP_{15}$, 388 kg/mol, in a mixture of 21%/79% (v/v) DMF-d_7/DMF (matching P4VP): red ▲, no water addition; black ▲, 1.3% water addition (matching P4VP); △, 3.8% water addition (matching P4VP). Solid lines are model fits.

DMF polymer solutions within the micelles and the surrounding semidilute PS/DMF solution, where $I_{0,2}$ and $I_{0,3}$ are the intensity coefficients and a_1 and a_2 are the correlation lengths of these semidilute solutions. For the data of PS-*b*-P4VP in DMF we were able to fit the model of eq 1. A good fit was obtained using $I_{0,1}$ = 78 cm^{-1}, R = 690 Å, $I_{0,2}$ = 5.9 cm^{-1}, a_1 = 53 Å, $I_{0,3}$ = 19 cm^{-1}, a_2 = 290 Å, and B = 0.09 cm^{-1}. When the solvent is contrast-matched to P4VP, the SANS patterns are simply fit by a model of a semidilute polymer solution (a single Lorentzian function plus constant in eq 1), as shown by the solid line in Figure 5. The fit parameters are $I_{0,2}$ = 9.1 cm^{-1}, a_1 = 69 Å, and B = 0.62 cm^{-1}. As DMF is a better solvent for P4VP, we expect these chains to be highly swollen, reflecting a high correlation length for the inner-micellar semidilute solution. The difference in the correlation length of the PS solutions is due to the difference in PS molecular weight and mole fraction between the copolymers used in full contrast and contrast-matching experiments. The main observation from these experiments is that the scattering from the micelles is eliminated by matching the scattering length density of the solvent to the hydrophilic polymer P4VP, proving that this polymer is in the micelle core.

The results presented in Figure 5 demonstrate formation of spherical micelles, with P4VP in their core, already at a copolymer concentration of 5% in DMF, in a solvent mixture of 70%/30% DMF/THF (see Supporting Information). Although DMF has a stronger interaction with P4VP than PS, the minority P4VP blocks form the core of the microphase-separated structure, while PS blocks are dissolved as a majority phase outside the micelles. The results presented here contradict the assumption presented in the literature for a very similar system: PS-*b*-P4VP copolymer membrane formed with complexation of copper ions.[9] In that work it was apparently wrongly assumed that micelles in solution are of PS cores and P4VP shells. Full analysis of the contrast-variation SANS measurements, including matching of the deuterated PS blocks, will be presented in a forthcoming publication.

To complement the SANS results with direct imaging, we prepared samples of similar solutions for cryo-TEM: 5% PS_{73}-*b*-$P4VP_{27}$, 310 kg/mol, in DMF. Imaging of the solution in the low-dose mode of the TEM showed little contrast between the copolymer blocks and between the copolymer and the solvent (Figure 6A). Contrast by mass−thickness and phase contrast due to variation in electron density, especially in hydrocarbon systems, is often not sufficient to provide detailed information

dx.doi.org/10.1021/ma301611c | *Macromolecules* 2012, 45, 9631−9642

on the spatial distribution of the different components of similar atomic makeup. However, controlled electron beam exposure during imaging can highlight structural features due to differences in the radiolysis pathway of the various components.[45−49] Indeed, after longer exposures of the sample to the electron beam, radiation damage occurred selectively, exposing spherical micelles (Figure 6B). This is due to differences in the sensitivity to electron-beam radiation damage between the core of the micelles and the solvent outside the micelle. The diameter of the micelles is around 45 nm, but they are not strictly monodisperse. The presence of spherical micelles in this solution is in agreement with the SANS results.

It is particularly relevant to this study that the interface between water and some organic matter is the site of extensive radiation sensitivity. Some polymers react differently to electron radiation and may either lose significant mass by radiolytic depolymerization (scission-type polymers) or densify by cross-linking,[46] as was applied to assess the structure of block copolymer latex particles.[49] Scission-type polymers become cellular in appearance, lose more mass, and occasionally swell, whereas cross-linking-type polymers are more stable under the beam. It is known from the literature that PS is a cross-linking-type polymer.[48] The more polar block, P4VP, was less studied, but it is known in general that more hydrophilic polymers tend to undergo radiolysis of the scission type.[49] Although most of these studies were done in vitrified or frozen water, not with organic solvents, our cryo-TEM results combined with SANS patterns show that here, too, the micelles core of the P4VP block is damaged by a scission-type reaction with the radiation of the electron beam. The PS block, dissolved in DMF as a shell in the outer part of the micelle, is less sensitive to the radiation damage. However, after longer exposure times, this part is also damaged by the electron beam. The solvent in the proximity of micelles (arrows in Figure 6B) is more sensitive to radiation damage than solvent in areas far from micelles (arrowheads) due to the free radicals produced while the micelle shells are irradiated.

Figure 7 shows that as small amounts of water (1.2% and 3.8%) were added to the copolymer solutions, a strong peak appeared in the SANS patterns. This peak became higher and shifted to lower angles with increased amounts of water, indicating formation of ordered structures of relatively large dimensions (tens of nanometers), as observed previously in different systems.[30,50,51] Similar peaks appeared for both the full contrast (Figure 7A) and the P4VP solvent-matched samples (Figure 7B), indicating that these ordered structures involve the PS blocks of the copolymer. The dramatic morphological changes induced by small additions of water were also indicated by visible changes of the solutions: the clear polymer solutions in DMF turned opaque immediately after addition of more than 0.5% water.

We were able to fit a model of spherical micelles (first part of eq 1, as the form factor) multiplied by a structure factor of hard spheres, for systems with more densely packed spheres with interparticle interferences.[52] Following Kinning and Thomas,[52] we allow the hard-sphere radius considered in the structure factor of inner-particle interactions to be larger than the sphere radius taken in the form factor. This accounts for the presence of a corona made of the shell blocks, providing an effective larger radius due to their hindrance of micellar contact. For the full contrast sample with 3.7% D_2O addition and for the copolymer with dPS polymer in solvent matched to P4VP with addition of 3.8% water (Figure 7), the model was fitted for spheres with the parameters specified in Table 1. The similarity of the values for model fitting of the full contrast and P4VP-matched samples indicate again that the spheres in this case are formed by the PS blocks, unlike the spheres in the samples without water addition.

Table 1. Model Fitting Parameters for 5% Copolymer Solutions[a]

sample	R, sphere radius (Å)	R_{hs}, effective hard sphere radius (Å)	hard spheres volume fraction
PS-*b*-P4VP in DMF-d_7	250	440	0.26
dPS-*b*-P4VP in DMF (matching P4VP)	310	510	0.26

[a]PS_{73}-*b*-$P4VP_{27}$, 310 kg/mol in DMF-d_7 (full contrast) with 3.7% D_2O addition; dPS_{85}-*b*-$P4VP_{15}$, 388 kg/mol, in a mixture of 21%/79% (v/v) DMF-d_7/DMF (matching P4VP) with 3.8% water addition (matching P4VP).

We visualized the influence of water addition on the structures in the system using cryo-TEM. Water was introduced into the system in three different ways. First, to observe the immediate, nonequilibrium, effect of water addition we exposed the sample to 100% relative humidity inside the CEVS, during cryo-TEM sample preparation (not shown). Second, we observed the same copolymer solutions in DMF, ∼1 h after addition of 1% (w) water. In both samples we observed mainly two kinds of morphologies: spherical micelles, similar to those observed in the samples that had not been exposed to humidity (Figure 6), and spherical micelles with cores less radiation sensitive than the solution and shells extremely stable to electron beam radiation (arrowheads in Figure 8B). Figures 8A and 8B show the same area of the sample after different electron beam exposures: ∼10 and ∼60 $e^-/Å^2$, respectively. Figure 8A shows little contrast between the copolymer blocks and between the copolymer and the solvent. The contrast is enhanced in Figure 8B due to the selective radiation damage.

Finally, we observed the 5% copolymer solution the day after addition of 5% (w) water. These samples were turbid, indicating the existence of larger-scale structures in the solution. Some of these undefined structures were observed by cryo-TEM (not shown). Smaller scale structures consisted of two different aggregates: spherical micelles similar to those shown in Figure 6 (not shown here), coexisting with core−shell spherical micelles shown in Figure 8C,D. The presence of the first kind of micelles indicated that the system still did not reach equilibrium. The latter kinds of micelles were almost invisible at first (Figure 8C) but became darker than their background after relatively high exposure to the electron beam (∼130 $e^-/Å^2$, Figure 8D). Their shells were darker than the background solution but lighter than their cores. In TEM, darker areas indicate higher mass−thickness. In this case it seems that the exposure to electron radiation led to cross-linking of the polymers inside the micelle, which increased its density. Another explanation may be different etching rates of different areas in the sample due to electron beam radiation, as shown by Thomas and Talmon.[45] Thus, the solution outside the micelles may have been etched faster, thus becoming lighter, than the micelle core during exposure to radiation. After comparing the electron intensity that passed through the sample in different areas after different exposure times, it seems that both processes happen in parallel: the micelle cores become denser and darker, while the solution outside them is etched and becomes lighter.

dx.doi.org/10.1021/ma301611c | Macromolecules 2012, 45, 9631−9642

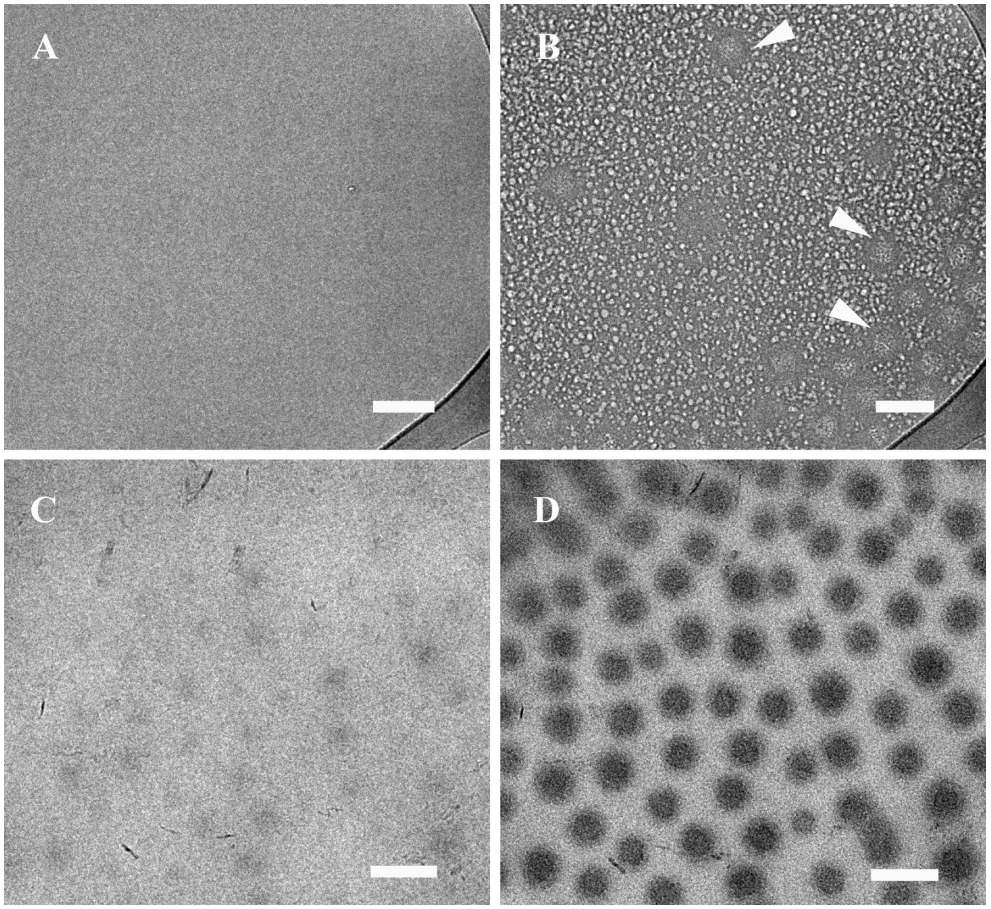

Figure 8. Cryo-TEM of 5% PS_{73}-*b*-$P4VP_{27}$, 310 kg/mol in DMF: ∼1 h after addition of 1% H_2O, with ∼10 $e^-/Å^2$ (A) or ∼60 $e^-/Å^2$; (B) electron beam exposure; 1 day after addition of 5% H_2O, with ∼10 $e^-/Å^2$; (C) or ∼130 $e^-/Å^2$ (D) electron beam exposure. Bars are 100 nm. Arrowheads show the stable collapsed shell around the micelles core.

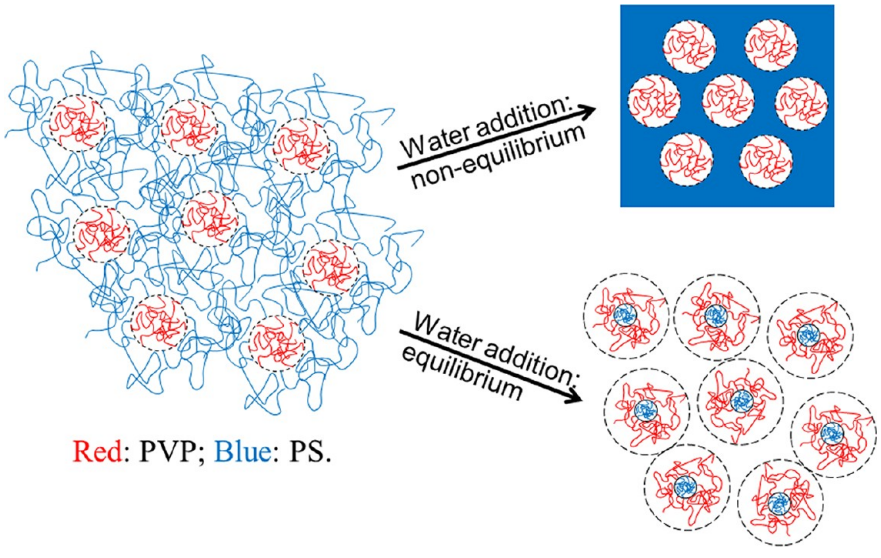

Figure 9. Schematic representation of the structures formed by addition of water to the P4VP-*b*-PS solution in DMF at equilibrium (lower arrow) and far from it (upper arrow).

The series of samples presented in Figures 6 and 8 show the effect of the addition of very small amounts of water to the copolymer solutions in DMF. The purpose of these experiments was to understand changes in the membrane surface as water is introduced during the membrane preparation process. In this step, since water is a nonsolvent of the copolymer, it is assumed that equilibrium is not reached, and the morphologies formed while the solvents evaporate are determined by the replacement of solvent with a nonsolvent.[7] The structures observed in Figure 8B may indicate the reaction of the system

dx.doi.org/10.1021/ma301611c | *Macromolecules* 2012, 45, 9631−9642

to first contact with water. In this case it was clear that equilibrium was not reached, since the solution still exhibited the same morphologies as in the original solution, before water addition: micelles (Figure 6), which probably contained some of the solvent in their cores. However, the second kind of micelles that appeared after small amounts of water entered the system (Figure 8B) indicated that as water was introduced, the more hydrophobic part of the copolymer (PS) collapsed from the swollen coiled state around the micelles into a dense shell that does not contain any solvent. Such a dense phase of PS is very stable under the electron beam. Hence, the solvent both outside the micelle shell and within its core was damaged, while the PS shell remained undamaged (arrowheads in Figure 8B). The third sample discussed above, mixed with 5% water 1 day before sample preparation, showed another step in the process between first contact with water and equilibrium (Figure 8C,D). Here we observed areas where the micelles aggregate together, with much less solvent in between micelles and inside them. This resulted in a different reaction to radiation exposure in these areas: instead of scission type reaction (as in Figure 6), we observed cross-linking type reaction, which is more typical for PS. The dominance of this reaction may be explained by two factors: the collapse of PS around the micelle core after water addition and PS being the majority part of the copolymer.

From these observations we can suggest two extreme cases for the structures formed in the block copolymer solution by addition of water, as shown schematically in Figure 9. At equilibrium, the initial solution is composed of micelles having P4VP in their core surrounded by a continuous phase of PS-rich semidilute solution. Rapid immersion in water, as in membrane casting, yields a nonequilibrium structure due to rapid collapse of the PS chains forming a shell around the micelles. This forms the continuous PS phase during membrane casting, as indicated by the top arrow in Figure 9. However, when water is slowly introduced, or sufficient time is provided, an equilibrium structure emerges in which the PS blocks form the micelle core and the P4VP block emanate into their surrounding good solvent.

An overview of all the results presented above, combined with models and data from the literature, lead to a possible model for pore self-assembly. Our model includes the following steps: (1) The copolymer solution contains mainly spherical micelles and short TLMs of P4VP cores with PS shells, both highly swollen with solvent. (2) As a thin film is cast, THF evaporation starts, causing spherical micelles on the top surface of the film to grow into TLMs. Because of fast evaporation, a result of the high vapor pressure of THF, this growth is oriented perpendicularly to the film surface.[15] (3) Solvent evaporation from deeper parts of the film is slower. Thus, nicely oriented cylinders form only at the top part of the membrane, whereas a sponge-like structure is formed underneath this top layer.[7] (4) As water is introduced into the system, the hydrophobic PS block of the copolymer tends to collapse around the micelles cores. In parallel, water tends to go inside the micelles core, where the more hydrophilic polymer remains, causing the cylinders to open and form pores. At this point the organic solvents are replaced by large water amount. (5) Since PS is the majority part of the copolymer, it forms a continuous phase around the pores. The inner side of the pores contains the P4VP block. This state is fixed due to the fast reaction of the system with water, far from equilibrium.

In the literature we found another model for membrane formation in the similar system of PS-*b*-P4VP copolymers, complexed with copper ions.[10,11] A significant assumption in that model, contradicted by the results presented here, is that micelles with PS cores and P4VP shells form the continuous part of the membrane, and such six standing TLMs are packed in a way that leaves an open pore between them. Our results show clearly that P4VP blocks form the core of the micelles already in solution and thus remain inside the membrane pores during casting, while the PS blocks that form the shells become the continuous phase.

CONCLUSIONS

The formation of uniform, nanometer-scale, hexagonally packed arrays of cylindrical pores on the surface of membranes provides substantial advantages of such membranes for various applications. The main goal of the work presented here was to investigate the structural transformations that are critical in the membrane formation process: casting of the block copolymer solution, solvent evaporation after film casting, and immersion into a nonsolvent (water). For this purpose we used a combination of direct imaging methods (room-temperature and cryogenic-temperature electron microscopy) with scattering methods (SANS). We have shown that the starting point for membrane formation is a micellar block copolymer solution with the hydrophilic minor blocks (P4VP) within the micelle core. As water is introduced, we found that this structure is preserved in a system that is far from equilibrium, as the PS blocks densify outside the more hydrophilic micelle cores. This nonequilibrium structure of hydrophilic micelle core may initiate further structural development in the membrane casting process, where cylindrical pores are formed as water continues to enter the system.[15] Conversely, slow addition of water, in a system that is closer to equilibrium, reverses the micellar structure so that the PS blocks form their core. To complete this model, we plan to conduct additional SANS experiments, including samples with lower water content, to show the initial effect of water on the system. We also plan to use cryo-HR-SEM to image structure formation after addition of water to the surface of the cast solution during membrane processing. Understanding the role of each parameter in the membrane casting process should allow better control over its characteristics, which may be better suited for specific applications.

ASSOCIATED CONTENT

Supporting Information

SANS patterns of 5% PS_{73}-*b*-$P4VP_{27}$, 310 kg/mol, copolymer solutions in DMF-d_7 and in a mixture of 30%/70% THF-d_8/DMF-d_7, both full contrast, presented together for comparison. This material is available free of charge via the Internet at http://pubs.acs.org.

AUTHOR INFORMATION

Corresponding Author

*E-mail: ishi@tx.technion.ac.il.

Notes

The authors declare no competing financial interest.

ACKNOWLEDGMENTS

The authors thank the European Commission for funding this work within the project SELFMEM (Grant Agreement NMP3-SL-2009-228652). We also thank Brigitte Lademann for the synthesis of the block copolymers. Sofia Rangou, Volkan Filz, and Daniel Fierro gave valuable information about the block

copolymers and the membrane preparation conditions. We thank Elinor Josef for her help with hard-sphere model fitting and Berta Shdemati for excellent technical assistance. The microscopy work was performed in the Technion Soft Matter Electron Microscopy Laboratory, supported by the Russell Berrie Nanotechnology Institute (RBNI). SANS measurements were supported by the European Commission seventh Framework Program Key Action: Strengthening the European Research Area, Research Infrastructures. Contract no. 283883 (NMI3-II).

REFERENCES

(1) Lodge, T. P.; Bang, J.; Li, Z.; Hillmyer, M. A.; Talmon, Y. *Faraday Discuss.* **2005**, *128*, 1−12.
(2) Hamley, I. W. *Block Copolymers in Solution: Fundamentals and Applications*; John Wiley & Sons, Ltd.: Chichester, 2005.
(3) Hayward, R. C.; Pochan, D. J. *Macromolecules* **2010**, *43*, 3577−3584.
(4) Albert, J. N. L.; Epps, T. H. *Mater. Today* **2010**, *13*, 24−33.
(5) Hillmyer, M. A. *Adv. Polym. Sci.* **2005**, *190*, 137−181.
(6) Jackson, E. A.; Hillmyer, M. A. *ACS Nano* **2010**, *4*, 3548−3553.
(7) Peinemann, K.-V.; Abetz, V.; Simon, P. F. W. *Nat. Mater.* **2007**, *6*, 992−996.
(8) Jung, A.; Rangou, S.; Abetz, C.; Filiz, V.; Abetz, V. *Macromol. Mater. Eng.* **2012**, *297*, 790−798.
(9) Nunes, S. P.; Sougrat, R.; Hooghan, B.; Anjum, D. H.; Behzad, A. R.; Zhao, L.; Pradeep, N.; Pinnau, I.; Vainio, U.; Peinemann, K.-V. *Macromolecules* **2010**, *43*, 8079−8085.
(10) Nunes, S. P.; Karunakaran, M.; Pradeep, N.; Behzad, A. R.; Hooghan, B.; Sougrat, R.; He, H.; Peinemann, K.-V. *Langmuir* **2011**, *27*, 10184−10190.
(11) Nunes, S. P.; Behzad, A. R.; Hooghan, B.; Sougrat, R.; Karunakaran, M.; Predeep, N.; Vainio, U.; Peinemann, K.-V. *ACS Nano* **2011**, *5*, 3516−3522.
(12) Park, S.; Wang, J.-Y.; Kim, B.; Xu, J.; Russell, T. P. *ACS Nano* **2008**, *2*, 766−772.
(13) Kim, S. H.; Misner, M. J.; Xu, T.; Kimura, M.; Russell, T. P. *Adv. Mater.* **2004**, *16*, 226−231.
(14) Phillip, W. A.; O'Neill, B.; Rodwogin, M.; Hillmyer, M. A.; Cussler, E. L. *ACS Appl. Mater. Interfaces* **2010**, *2*, 847−853.
(15) Phillip, W. A.; Hillmyer, M. A.; Cussler, E. L. *Macromolecules* **2010**, *43*, 7763−7770.
(16) Mulder, M. *Basic Principles of Membrane Technology*, 2nd ed.; Kluwer Academic Publishers: Dordrecht, 1996; pp 89−117.
(17) Barth, C.; Goncalves, M. C.; Pires, A. T. N.; Roeder, J.; Wolf, B. *J. Membr. Sci.* **2000**, *169*, 287−299.
(18) Lodge, T. P.; Pudil, B.; Hanley, K. J. *Macromolecules* **2002**, *35*, 4707−4717.
(19) Park, M. J.; Char, K.; Bang, J.; Lodge, T. P. *Macromolecules* **2005**, *38*, 2449−2459.
(20) Mukamel, D. In *Soft and Fragile Matter*; Cates, M. E., Evans, M. R., Eds.; Scottish Universities Summer School in Physics & Institute of Physics Publishing: Bristol, 2000; pp 237−258.
(21) Talmon, Y. *Ber. Bunsenges. Phys. Chem.* **1996**, *100*, 364−372.
(22) Talmon, Y. In *Modern Characterization Methods of Surfactant Systems*; Binks, B. P., Ed.; Marcel Dekker: New York, 1999; pp 147−178.
(23) Issman, L.; Talmon, Y. *J. Microsc.* **2012**, *246*, 60−69.
(24) Lodge, T. P.; Hanley, K. J.; Pudil, B.; Alahapperuma, V. *Macromolecules* **2003**, *36*, 816−822.
(25) Pedersen, J. S.; Svaneborg, C. *Curr. Opin. Colloid Interface Sci.* **2002**, *7*, 158−166.
(26) Pedersen, J. S. *Adv. Colloid Interface* **1997**, *70*, 171−210.
(27) Mortensen, K. *Polym. Adv. Technol.* **2001**, *12*, 2−22.
(28) Ando, K.; Yamanaka, T.; Okamoto, S.; Sakamoto, N.; Yamaguchi, D.; Koizumi, S.; Hasegawa, H.; Koshikawa, N. *J. Phys.: Conf. Ser.* **2010**, *247*, 012040.
(29) Lodge, T. P.; Hamersky, M. W.; Hanley, K. J.; Huang, C.-I. *Macromolecules* **1997**, *30*, 6139−6149.
(30) Ando, K.; Yamanaka, T.; Okamoto, S.; Inoue, T.; Sakamoto, N.; Yamaguchi, D.; Koizumi, S.; Hasegawa, H.; Koshikawa, N. *IOP Conf. Ser.: Mater. Sci. Eng.* **2010**, *14*, 012012.
(31) Danino, D.; Gupta, R.; Satyavolu, J.; Talmon, Y. *J. Colloid Interface Sci.* **2002**, *249*, 180−186.
(32) Danino, D.; Bernheim-Groswasser, A.; Talmon, Y. *Colloids Surf., A* **2001**, *183*−*185*, 113−122.
(33) Fierro, D.; Buhr, K.; Abetz, C.; Boschetti-de-Fierro, A.; Abetz, V. *Aust. J. Chem.* **2009**, *62*, 885−890.
(34) Bates, F. S.; Fredrickson, G. H. *Phys. Today* **1999**, *52*, 32−38.
(35) Bernheim-Groswasser, A.; Zana, R.; Talmon, Y. *J. Phys. Chem. B* **2000**, *104*, 4005−4009.
(36) Zheng, Y.; Won, Y.-Y.; Bates, F. S.; Davis, H. T.; Scriven, L. E.; Talmon, Y. *J. Phys. Chem. B* **1999**, *103*, 10331−10334.
(37) Cardinal, C. M.; Francis, L. F.; Scriven, L. E. *J. Coat. Technol. Res.* **2009**, *6*, 457−469.
(38) Zhang, L.; Eizenberg, A. *J. Am. Chem. Soc.* **1996**, *118*, 3168−3181.
(39) Park, S.-Y.; Sul, W.-H.; Chang, Y.-J. *Macromolecules* **2007**, *40*, 3757−3764.
(40) Capone, B.; Hansen, J.-P.; Coluzza, I. *Soft Matter* **2010**, *6*, 6075−6078.
(41) Reddy, C. R.; Kashyap, A. K.; Klapagam, V. *Polymer* **1977**, *18*, 32−36.
(42) Daoud, M.; Cotton, J. .; Farnoux, B.; Jannink, G.; Sarma, G.; Benoit, H.; Duplessix, R.; Picot, C.; DeGennes, P. G. *Macromolecules* **1975**, *8*, 804−818.
(43) Higgins, J. S.; Benoit, H. C. *Polymers and Neutron Scattering*; Oxford University Press Inc.: New York, 1994.
(44) Bianco, H.; Narkis, M.; Cohen, Y. *J. Appl. Crystallogr.* **1998**, *31*, 369−372.
(45) Thomas, E. L.; Talmon, Y. *Polymer* **1978**, *19*, 225−227.
(46) Talmon, Y. *Ultramicroscopy* **1984**, *14*, 305−316.
(47) Silverstein, M. S.; Talmon, Y.; Narkis, M. *Polymer* **1989**, *30*, 416−424.
(48) Narkis, M.; Talmon, Y.; Silverstein, M. *Polymer* **1985**, *26*, 1359−1364.
(49) Haas-Bar Ilan, A.; Noda, I.; Schechtman, L. A.; Talmon, Y. *Polymer* **1992**, *33*, 2043−2050.
(50) Fuse, C.; Okabe, S.; Sugihara, S.; Aoshima, S.; Shibayama, M. *Macromolecules* **2004**, *37*, 7791−7798.
(51) Peng, J.; Xuan, Y.; Wang, H.; Yang, Y.; Li, B.; Han, Y. *J. Chem. Phys.* **2004**, *120*, 11163−11170.
(52) Kinning, D. J.; Thomas, E. L. *Macromolecules* **1984**, *17*, 1712−1718.